AJNR

MR Spectroscopy of Bilateral Thalamic Gliomas

François Estève, Sylvie Grand, Christophe Rubin, Dominique Hoffmann, Basile Pasquier, Danielle Graveron-Demilly, Rachid Mahdjoub and Jean-François Le Bas

AJNR Am J Neuroradiol 1999, 20 (5) 876-881
http://www.ajnr.org/content/20/5/876

AJNR Am J Neuroradiol 20:876–881, May 1999

Case Report

MR Spectroscopy of Bilateral Thalamic Gliomas

François Estève, Sylvie Grand, Christophe Rubin, Dominique Hoffmann, Basile Pasquier, Danielle Graveron-Demilly, Rachid Mahdjoub, and Jean-François Le Bas

Summary: This study reports the MR spectroscopic patterns of two patients with bithalamic glioma. In one patient, phosphorus (^{31}P) MR spectroscopy was performed. In both patients, the proton MR spectroscopic scans showed an increased creatine-phosphocreatine peak in the tumor. In the patient who underwent ^{31}P-MR spectroscopy, an increased phosphocreatine peak was also observed. This group of thalamic tumors may be distinguished from other gliomas clinically, radiologically, and metabolically.

Among the primary thalamic gliomas, a type known as bilateral thalamic glioma (BTG) has been identified (1–3) in which a large tumor appears symmetrically in both thalami and is accompanied by behavioral impairments varying from personality changes to dementia (3). In a 1938 study of tumors of the thalamus, Smyth and Stern (1) described a group of tumors originating from the subependymal glia of the third ventricle that led to the development of bilateral symmetric tumors. We present the findings in two patients with BTG, as defined on clinical and radiologic examinations, and describe the unusual MR spectroscopic patterns of these gliomas.

Case Reports and Description of the Technique

Case 1

A 31-year-old man with no significant familial medical history presented with allergic rhinitis, of several years' duration and a dramatic loss of visual acuity accompanied by strong, continuous headaches, which had developed 2 months before admission. Clinical examination showed a left-sided hemianopsia and a dramatic loss of visual acuity. The fundus showed bilateral papillary edema. No sensory or motor deficit was found. The patient had noted significant behavioral changes during the weeks before the first examination, including unusual emotional instability, difficulty concentrating, and loss of interest. A stereotactic biopsy was performed, and two ventricular shunts were connected to the peritoneal cavity. Neurohistologic analysis of the biopsy material led to the diagnosis of glioma grade II (World Health Organization [WHO], 1993).

Radiotherapy was initiated, with an overall dose close to 60 Gy in the tumoral area delivered in 35 exposures over 50 days. After 8 months of clinical stability, the patient's severe headaches resumed and his deteriorating consciousness led to coma and death.

Case 2

A 21-year-old man presented with a dramatic loss of visual acuity. A year earlier, he had begun to lose his usual sleeping and eating rhythms, and at times he was hyperphagic. He noted a progressive loss of interest, emotional disturbances, and difficulty concentrating. He was anosognosic, had memory troubles, and difficulty reading. On physical examination, a dramatic loss of visual acuity was discovered, and the fundus showed large bilateral papillary edema. Neurohistologic analysis of a biopsy specimen led to the diagnosis of glioma grade II (WHO, 1993) (Fig 1). He was treated in the same way as patient 1, with the same schedule and dose of radiation therapy. Five months after the consultation, he became mute and akinetic; however, this motor slowness disappeared 4 months later. At the time of this writing, the patient's neuropsychological condition is improved.

Technique

Both patients underwent MR imaging, including noncontrast and contrast-enhanced sagittal and coronal T1-weighted spin-echo sequences with parameters of 550/15/2 (TR/TE/excitations) and a 6-mm section thickness with a 0.6-mm intersection gap, and axial T2-weighted turbo spin-echo sequences (3900/100/4) (Fig 2). MR imaging and MR spectroscopic studies were done on a 1.5-T whole-body imager with the standard imaging and spectroscopy software. Both MR imaging and MR spectroscopic studies were performed before and 3 months after the patients had radiation therapy. The regular proton spectroscopy quadrature head coil was used for both excitation and signal detection. The volume of interest (VOI) for proton MR spectroscopic measurements was selected on the basis of T2-weighted turbo spin-echo images acquired in the axial orientation. Water-suppressed proton MR spectroscopy was done with a point-resolved spectroscopic (PRESS) sequence with parameters of 1500/272/1 and a scan time of 10 minutes 42 seconds. Typical VOI dimensions were 100, 90, and 20 mm in the anteroposterior, left-right, and craniocaudal directions, respectively. Angulation in the anteroposterior direction was chosen to make the VOI parallel to the bicommissural line of Talairach (anterior commissure-posterior commissure) (Fig 2). The number of steps for phase encoding was limited to 16 in both the anteroposterior and left-right directions. The field of view was 160×160 mm^2, resulting in a nominal voxel size on the spectroscopic image of $10 \times 10 \times 20$ mm^3. The typical proton MR spectroscopic scan lasted 30 minutes. Signal processing of spectroscopic raw data, including peak area determination by gaussian curve fitting, was carried out with in-

Received June 22, 1998; accepted after revision January 20, 1999.

Supported by the Ministère de la Santé, and Biomedical Technology and Engineering EC contract PL950861.

From the Unité IRM (F.E., S.G., J-F.L.B.), the Unité INSERM 438, University Joseph Fourier (F.E., S.G., C.R., J-F.L.B.), the Service de Neurochirurgie (D.H.), and the Service d'Anatomie Pathologique (B.P.), Centre Hospitalier Universitaire de Grenoble; and the Laboratoire RMN CNRS UPRESA 5012 UCB Lyon (D.G-D., R.M.), France.

Address reprint requests to François Estève, MD, PhD, Unité IRM, Centre Hospitalier Universitaire de Grenoble, BP 217 38043 Grenoble Cedex 9, France.

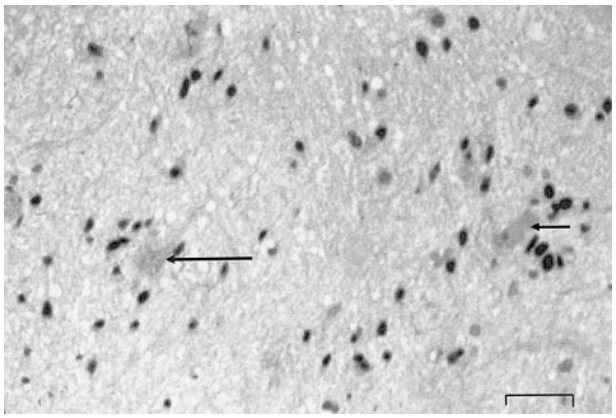

FIG 1. Histopathologic section from biopsy sample obtained in patient 2. A few neuronal cells are visible (*arrows*), surrounded by astrocytes with hyperchromatic nuclei in a fibrillar eosinophilic background. Immunohistochemical study has shown that the tumoral cells express the GFA protein; the KI-67 index was low. No necrosis or mitotic figures or endothelial proliferation were observed. These elements are consistent with the diagnosis of astrocytoma grade II (WHO, 1993). Scale bar: 60 μm. Hematoxylin erythrosin saffron.

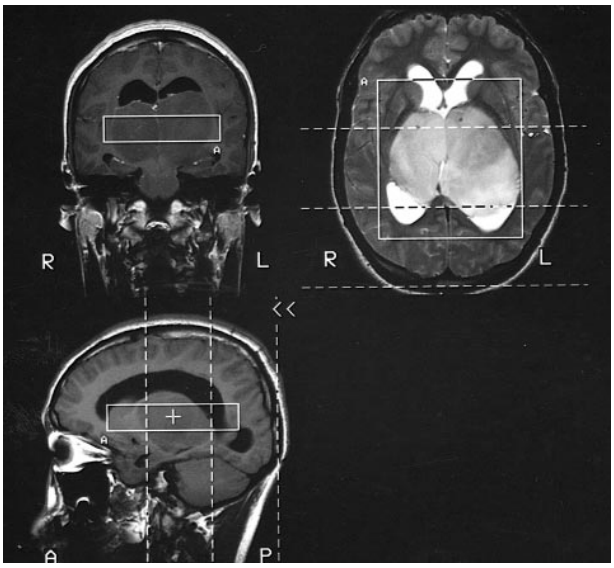

FIG 2. MR images of the BTG in patient 1.

Upper and Lower Left, T1-weighted MR images of a large tumoral mass, including both thalami. Lateral ventricles are expanded owing to the obstruction of the interventricular foramen.

Upper Right, T2-weighted MR image in axial orientation shows the tumoral mass infiltrating both thalami and the head of the caudate nucleus. The VOI for the proton MR spectroscopic image was located by using the three orientations and included a large amount of tumoral tissue.

house software. The raw-data processing is described elsewhere (4). For each metabolite, we made a 16 $\times$ 16 map of the selected brain section, with each pixel gray level corresponding to a peak area. These maps were adjusted to 256 $\times$ 256 by Fourier interpolation, resulting in metabolic images of the brain section, with each pixel gray level proportional to the interpolated value of the corresponding metabolite peak area (Fig 3A).

Tumoral and healthy regions of interest (ROI) were selected on the T2-weighted turbo spin-echo MR images and transferred to the metabolic images. The mean peak area was then calculated in each ROI. Because both thalami were invaded, it was not possible to compare tumoral and healthy volumes in the same contralateral regions. This is shown in (Fig 3B), where tumoral and healthy ROIs are drawn for patient 1. The normalized values of each peak area in a given ROI were obtained by dividing the averaged peak area of the metabolite of interest by the sum of the peak areas of all the metabolites in the ROI. These normalized values (NV) for the peak areas were called $NAA_{(NV)}$, $Cho_{(NV)}$, $Cr_{(NV)}$, and $Lac_{(NV)}$ for *N*-acetylaspartate, choline, creatine, and lactate, respectively. We defined ratios of the intensity of each metabolite in the tumoral ROI to the intensity of NAA in the healthy ROI as $Cr_{(t)}/NAA_{(h)}$, $Cho_{(t)}/NAA_{(h)}$, and $Lac_{(t)}/NAA_{(h)}$. Finally, to compare Cr intensity in tumoral and healthy ROIs, we calculated the ratio $Cr_{(t)}/Cr_{(h)}$.

Owing to the dependence of metabolic intensity on brain region and age (5), reference values from normal brain tissue were obtained in the thalami of a group of 10 healthy volunteers (average age, 36 $\pm$ 12 years). To compare ratios obtained in tumoral regions in our patients with those obtained in other gliomas, reference values were also obtained from 14 patients with grade II and I (WHO) gliomas (average age, 37 $\pm$ 12 years).

To complement the proton MR spectroscopic study concerning the Cr-PCr MR spectroscopic signal, patient 2 underwent ^{31}P MR spectroscopy. The VOI for ^{31}P MR spectroscopic measurements was selected on the basis of T2-weighted turbo spin-echo MR images obtained with the whole-body coil. Using the phosphorus quadrature head coil for excitation as well as for reception, we obtained a single spectrum in a 50 $\times$ 73 $\times$ 42 mm^3 (anteroposterior, left-right, craniocaudal direction, respectively) volume containing the tumor. Acquisition was run using an image-selected in vivo spectroscopic (ISIS) sequence (TR, 3000; excitations, 384; scan time, 20 minutes). Time-domain signals were processed with the MRUI package (http://mrui.uab.es/mrui971/mrui HomePage.html), peaks were assigned with PCr set to 0 ppm as a chemical-shift reference, and the amplitudes of metabolites were quantified with the VARPRO method (6). Prior knowledge about adenosine triphosphate (ATP) multiplet structures was included in the fit. The noise-related errors on amplitudes were estimated with the Cramer-Rao theory (7). The pH was determined by the chemical shift between the inorganic phosphate (Pi) and PCr resonances, with the formula taken from Ng et al (8) to assess the Pi to PCr separation as a function of the pH. Peak area measurements were expressed in normalized values relative to $P_{tot}/100$; that is, as a percentage of the total peak areas in the spectrum. Reference values were obtained from a second group of seven healthy volunteers (average age, 34 $\pm$ 11). To minimize the variability of the measurements, scans were done with the same MR spectroscopy sequence, VOI location and size, and raw data processing.

The values obtained from both BTGs with phosphorus and proton MR spectroscopy were compared with those obtained in the two groups of volunteers. One group included 10 volunteers for the proton MR spectroscopy reference values, and the other group included seven volunteers for the ^{31}P MR spectroscopy reference values. The proton MR spectroscopy values for the BTGs were compared with those observed in the grade I and II glioma group. We assumed a gaussian distribution for the values from the different groups, and set the confidence interval to 99% (mean $\pm$ 2.57 SD) for all data analysis. Informed consent was obtained from each patient and volunteer.

T2-weighted images clearly showed two dramatically enlarged hyperintense thalami. Neuropathologic examination of the stereotactic biopsy samples, however, did not reveal any difference between BTG and other similar-grade gliomas.

Discussion

In both patients, MR images showed large tumors entirely occupying each thalamus. For patient

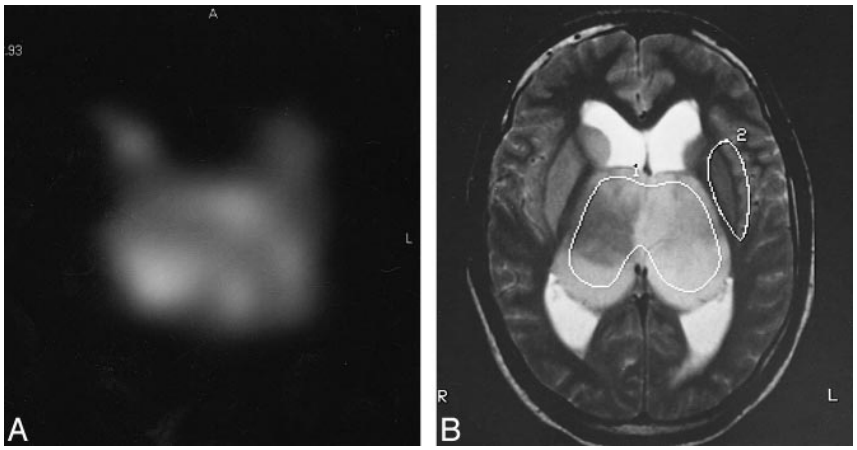

FIG 3. *A,* MR spectroscopic image of the Cr-PCr interpolated peak area values (see text). The highest level of the Cr-PCr MR spectroscopic signal appears on the right side of the tumor.

B, Tumoral (*1*) and normal (*2*) areas used for metabolic analysis are drawn on this T2-weighted MR image obtained from patient 1.

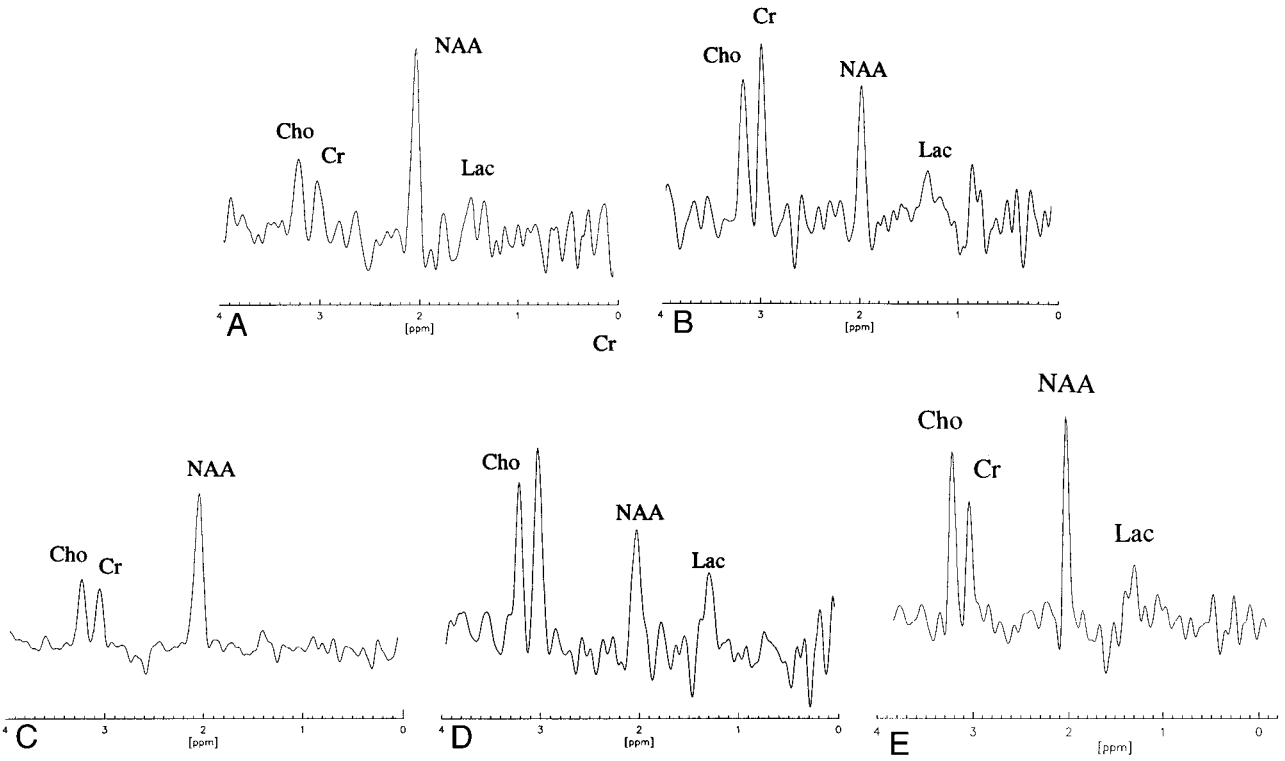

FIG 4. *A–E,* Comparison patterns of proton spectrum for both patients with BTG (patient 1, *A* and *B*; patient 2, *C* and *D*) obtained from voxels in normal areas (*A* and *C*) and tumoral areas (*B* and *D*) with peak assignments. The Cr peak is higher than the Cho peak in tumoral areas. These unusual patterns are different from that usually observed in a low-grade glioma (*E*). The 1.3 ppm resonance has been assigned to Lac in all spectra.

1, there was a spread on the right side to the head of the caudate nucleus (Fig 2). For both patients, we observed unusual spectra in tumoral regions on the first proton MR spectroscopic scan. The patterns differed from those observed in healthy brain tissue as well as from those usually observed in patients with low-grade gliomas. In both BTG patients, the Cr peak appeared to be greater than the Cho peak in the tumor, in contrast to the increased MR Cho signal usually observed in low-grade gliomas (Fig 4). The MR NAA signal was decreased in both BTGs, as is usually observed in low-grade gliomas. The various metabolic ratios for both patients are listed in Table 1. For comparison, we also list the same ratios for patients with grade I and II gliomas and for the volunteers. The changes observed in various ratios involving Cr were consistent with an increased Cr MR signal. $Cr_{(t)}/NAA_{(h)}$ and $Cr_{(NV)}$ were dramatically higher (outside the 99% confidence interval) in both patients with BTG relative to the group with low-grade gliomas. Furthermore, the $Cr_{(NV)}$ was approximately twice the normal reference value. The ratios $Cr_{(t)}/Cr_{(h)}$ for patients with BTG were greater than the average value observed in patients with low-grade gliomas (1.44 and 1.36 versus 0.945 ± 0.29, $n = 14$), but, owing to the great variability of this ratio in the grade I and II glioma group,

TABLE 1: Metabolite comparison between bilateral thalamic gliomas and other low-grade gliomas*

	Bilateral Thalamic Gliomas		Gliomas Grade I and II (n = 14)	Normal Reference Values (n = 10)	
	Patient 1	Patient 2			
Ratios (tumoral/healthy)					
$Cr_{(t)}/NAA_{(h)}$	0.57† *(0.52)*	0.57† *(0.52)*	0.22 ± 0.1	Cr/NAA	0.22 ± 0.02
$Cho_{(t)}/NAA_{(h)}$	0.64 *(0.42)*	0.53 *(0.41)*	0.40 ± 0.09	Cho/NAA	0.29 ± 0.04
$Lac_{(t)}/NAA_{(h)}$	0.35 *(0.14)*	0.52 *(0.16)*	0.18 ± 0.10		
$Cr_{(t)}/Cr_{(h)}$	1.44 *(1.25)*	1.36 *(1.36)*	0.94 ± 0.3		
$NAA_{(t)}/NAA_{(h)}$	0.40 *(0.39)*	0.70 *(0.54)*	0.54 ± 0.22		
Normalized values					
$NAA_{(t)\ (NV)}$	0.29 *(0.26)*	0.22 *(0.33)*	0.38 ± 0.1	$NAA_{(NV)}$	0.67 ± 0.02
$Cho_{(t)\ (NV)}$	0.29 *(0.28)*	0.29 *(0.25)*	0.30 ± 0.06	$Cho_{(NV)}$	0.19 ± 0.02
$Cr_{(t)\ (NV)}$	0.26† *(0.35)*	0.31† *(0.32)*	0.17 ± 0.03	$Cr_{(NV)}$	0.14 ± 0.01
$Lac_{(t)\ (NV)}$	0.13 *(0.09)*	0.19 *(0.10)*	0.14 ± 0.09	$Lac_{(NV)}$	≈0

Note.—Cho indicates choline-containing compounds; NAA, *N*-Acetyl aspartate; Cr, creatine-phosphocreatine; Lac, lactate; (h) and (t) indicate whether measurements are done in healthy (h) brain tissue or in tumoral (t) tissue. Statistical analysis concerns comparisons between the first proton MR spectroscopic scan for both patients and for the patients with low-grade glioma.

* Values in parentheses and italics are from MR spectroscopic study done 3 months later, after radiation therapy.

† Value outside the 99% confidence interval (mean ± 2.57 SD) compared with low-grade gliomas.

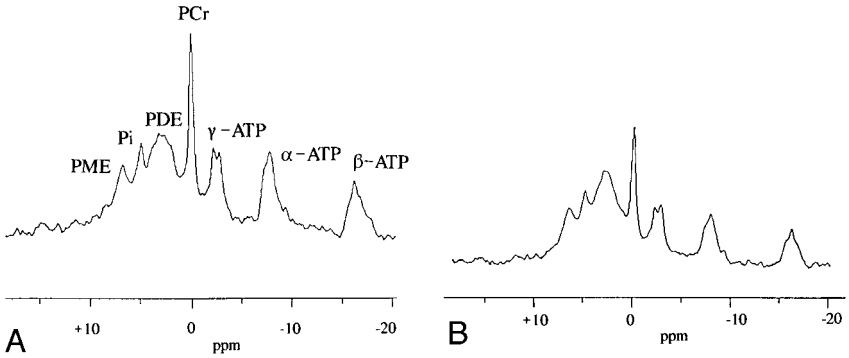

FIG 5. *A* and *B*, Phosphorus spectrum in single VOI ISIS sequence obtained in patient 2 (*A*). The PCr peak is higher than in a spectrum obtained under the same conditions in a healthy volunteer (*B*). *PDE* indicates phosphodiester; *PME*, phosphomonoester.

they were within the 95% confidence interval. Three months later, for both patients, the second MR spectroscopic scan yielded similar results for the $Cr_{(NV)}$ and Cr ratios (Table 1).

For the second patient, the ^{31}P MR spectrum showed a higher phosphocreatine (PCr) peak than was found in the healthy volunteer group (Fig 5). Table 2 lists the data derived from ^{31}P MR spectroscopy in the healthy volunteer group and in patient 2. The pH measured in the VOI on the ^{31}P MR spectroscopic image was 7.12 for this patient, close to the mean value for the healthy volunteer group (7.06 ± 0.05, n = 7). The pH of this BTG agreed with the values reported in the literature on brain tumors (9). When normalized to $P_{tot}/100$, the PCr was significantly higher (confidence interval set to 99%) for patient 2 relative to values in the volunteer group (10.4 versus 6.92 ± 1.09, n = 7).

Thalamic tumors make up 1% to 1.5% of brain tumors (2). BTG is rare among the thalamic tumors (3) and has a very poor prognosis, despite therapy. The largest previous study followed eight cases of BTG observed during 18 years, starting in 1963 (3). Mental deterioration was presumed to be due to direct interaction of the tumor on the thalamus. McKissock and Paine (2) thought that behavioral disorders and intellectual impairment were due only to raised intracranial pressure. In both our cases, mental impairment was consistent with related thalamic disorders, as observed in cases of glioma in medial areas of the thalamus (1, 3). Similar impairments have also been reported in asso-

TABLE 2: Metabolic and pH values with phosphorus MR spectroscopy

	Volunteer group n = 7	Patient 2
PME	5.92 ± 3.8	10.66
PI	3.43 ± 1.05	3.00
PDE	48.74 ± 3.10	44.03
PCr	6.92 ± 1.09	10.40*
γ-ATP	7.87 ± 0.92	10.14
α-ATP	10.18 ± 1.47	13.15
β-ATP	8.04 ± 1.74	9.97
pH	7.06 ± 0.05	7.12

Note.—PME indicates phosphomonoester; PI, inorganic phosphate; PDE, phosphodiester; PCr, phosphocreatine; ATP, adenosine triphosphate. Values are mean ± SD.

* Value outside the 99% confidence interval (mean ± 2.57 SD) as compared with the corresponding measurements in the healthy volunteer group.

ciation with thalamic functions in a case report by Stern (10) of severe dementia associated with bilateral symmetric degeneration of the thalamus, and in one by Smyth and Stern (1) of a thalamic glioma. These authors differentiated two types of thalamic gliomas on the basis of the area from which they came. In group I, the tumor originates in the peduncular and capsulothalamic areas and invades the lateral or ventrolateral thalamus, leading to sensory disturbances at an early stage of the disease. In group II, which the authors called intrinsic thalamic gliomas, the tumor originates in the subependymal glia in the third ventricle and expands laterally from the medial nuclei, leading to early mental deterioration. In the early stage, these tumors had the tendency to stop at the margins between gray and white matter. These features were indeed observed on the MR images of both our patients with BTG.

Because of their symmetric appearance on MR images, it is likely that BTGs originate in or near the central area, spreading to both thalami via the interthalamic adhesion. In this sense, and in their anatomoclinical features, the BTGs that we observed are a special case of group II intrinsic thalamic gliomas.

MR spectroscopy with both phosphorus and proton nuclei offers metabolic insight into tumoral and healthy brain tissue. The proton MR spectroscopic NAA signal (2.02 ppm) is considered a marker of neuronal tissue, whereas the proton MR spectroscopic Cho signal (3.2 ppm) is correlated with cell membrane biosynthesis and with Cho turnover, especially in proliferating tissue (11, 12). The proton MR spectroscopy Cr signal (3.02 ppm) is caused by both Cr and PCr, metabolites involved in cellular energetics (11, 12). A PCr peak may be observed with ^{31}P MR spectroscopy.

Both our cases of BTG had unusual MR spectroscopic patterns. To our knowledge, such significant increases in the MR spectroscopy Cr signal have not been reported before, nor have we observed such a pattern in any other type of brain tumor. To the contrary, the Cr-PCr MR signal is either lower or nearly unchanged in low-grade gliomas as compared with normal brain tissue (13). The increase of the PCr MR signal on the ^{31}P spectrum of patient 2 reinforced the singular appearance of the proton MR spectroscopy data obtained in patients 1 and 2. Phosphorus spectra in grade II gliomas are usually similar to those of normal brain (9, 14). According to other authors, a decreased peak of PCr is often observed in brain tumors (15).

Our sample of only two cases of BTG is a limitation of this study. On the other hand, spectroscopic singularities were observed over large areas in both cases, and were still observed after radiation therapy, reinforcing the original aspect of the initial MR spectroscopy data.

What caused the increased level of Cr-PCr (at proton MR spectroscopy) and PCr (at ^{31}P MR spectroscopy)? This question will have to be answered in future studies. Our findings suggest that these tumors have a unique metabolism, whose complete analysis may be of interest. MR spectroscopic findings reinforced the concept of a peculiar group of thalamic tumors, as already suggested by Smyth and Stern (1), and suggested that these tumors have an unusual metabolism.

Conclusion

Metabolic analysis of two cases of BTG by MR spectroscopy showed a higher Cr-PCr signal than normal reference values and than observed in low-grade gliomas. In one patient, ^{31}P MR spectroscopy showed a higher level of PCr than found in a volunteer group. These original patterns seen with MR spectroscopy lend new support to the concept of a specific group of brain gliomas, and of thalamic tumors in particular.

Acknowledgments

We are grateful to S. Cavassila (Laboratoire RMN CNRS, Lyon) for her help in phosphorus spectrum processing with the MRUI software package. The MRUI software package was kindly provided by the groups involved in the EC projects HCM-CHRX-CT94-0432 and TMR ERBFMRXCT970160. We are grateful to Denis Downes for his helpful advice on the manuscript. We thank the patients and the volunteers for their cooperation and the team of the MRI unit for their help.

References

1. Smyth EG, Stern K. **Tumors of the thalamus: a clinico-pathological study.** *Brain* 1938;61:339–374
2. McKissock W, Paine KWE. **Primary tumors of the thalamus.** *Brain* 1958;81:41–63
3. Partlow GD, O'Donovan R del C, Melanson D, Peters TM. **Bilateral thalamic glioma: review of eight cases with personality change and mental deterioration.** *AJNR Am J Neuroradiol* 1992; 13:1225–1230
4. Estève F, Rubin C, Grand S, Kolodié H, Le Bas JF. **Transient metabolic changes observed with proton MR spectroscopy in normal human brain after radiation therapy.** *Int J Radiat Oncol Biol Phys* 1998;40:279–286

5. Christiansen P, Toft P, Larsson HBW, Stubgaard M, Henriksen O. **The concentration of N-acetyl aspartate, creatine + phosphocreatine, and choline in different parts of the brain in adulthood and senium.** *Magn Reson Imaging* 1993;11:799–806
6. De Beer R, Van Ormondt D. **Analysis of NMR data using time domain fitting methods.** In: Diehl P, Fluck E, Günther H, Kosfeld R, Feelig J, eds. *NMR Basic Principles and Progress.* Berlin: Springer; 1992:202–248
7. van den Bos A, Cramer-Rao A. **Lower bound for complex parameter.** *IEEE Trans Signal Proc* 1994;42:–2859
8. Ng T, Majors AW, Vijayakumar S, et al. **Human neoplasm pH and response to radiation therapy: P-31 MR spectroscopy studies in situ.** *Radiology* 1989;170:875–878
9. Segebarth CM, Baleriaux DF, De Beer R, et al. **^{1}H image guided localized ^{31}P-MR spectroscopy of human brain: quantitative analysis of ^{31}P-MR spectra measured on volunteers and on intracranial tumor patients.** *Magn Reson Med* 1989;11:349–366
10. Stern K. **Severe dementia associated with bilateral symmetrical degeneration of the thalamus.** *Brain* 1939;62:157–171
11. Luyten PR, Marien Ad JH, Heindel W, et al. **Metabolic imaging of patients with intracranial tumors: ^{1}H-MR spectroscopic imaging and PET.** *Radiology* 1990;176:791–799
12. Williams SR. **In vivo proton spectroscopy: experimental aspects and potential.** In: Diehl P, Fluck E, Günther H, Kosfeld R, Feelig J, eds. *NMR Basic Principles and Progress.* Berlin: Springer; 1992:55–70
13. Kuggel H, Heindel W, Ernestus RI, Bunke J, Du Mesnil R, Friedmann G. **Human brain tumors: spectral patterns detected with localized ^{1}H-MR spectroscopy.** *Radiology* 1992;183:701–709
14. Heiss WD, Heindel W, Herholz K, Bunke J, Jeske J, Friedmann G. **Positron emission tomography of fluorine-18-deoxyglucose and image-guided phosphorus-31 magnetic resonance spectroscopy in brain tumors.** *J Nucl Med* 1990;31:302–310
15. Asakura T, Sasahira M. **Magnetic resonance spectroscopy and chemical shift imaging of the brain.** *Neurosciences* 1994;20:83–101